IEEE Access
Multidisciplinary | Rapid Review | Open Access Journal

Received August 19, 2020, accepted August 23, 2020, date of publication August 26, 2020, date of current version September 22, 2020.

Digital Object Identifier 10.1109/ACCESS.2020.3019713

Inversion of Smoke Black Concentration Field in a Tangentially Fired Furnace Based on Super-Resolution Reconstruction

ZHENHUA WEI, YUQI WANG, ZHIHONG LI, AND LING ZHENG
School of Control and Computer Engineering, North China Electric Power University, Beijing 102200, China
Corresponding author: Yuqi Wang (1182227208@ncepu.edu.cn)

ABSTRACT The tangentially fired furnace has the advantages of sufficient combustion and low NOx emission, and the smoke black concentration in the furnace reflects the combustion situation of combustion equipment. The flame field and smoke black concentration field in the furnace are complex, so it is meaningful to study the flame field and the smoke black concentration field of the tangential furnace. In this article, the visual method was used to reconstruct the flame and smoke black concentration fields in the furnace. Due to the low resolution of industrial cameras, the final reconstruction effect is limited. Given this situation, this article proposes a strengthen edge characteristic super-resolution network (SECSR) algorithm suitable for the tangentially fired furnace flame images. The flame edge processing is added to the depth neural network, which enhances the ability of flame edge feature extraction. It constructs a generative adversarial network which can greatly improve the resolution of furnace flame image, to obtain high-resolution tangential furnace flame image. Secondly, based on the high-quality flame image, this article proposes an inversion algorithm of the black concentration field of the tangentially fired furnace smoke. The algorithm obtains the high-precision tangentially furnace flame temperature field through an inversion calculation to calculate the soot concentration field. In the future work, we will predict the variation trend of smoke black concentration in the furnace through the results of the inversion calculation model, to understand the combustion situation in the furnace and control the fuel consumption to reduce smoke black emission, which has important guiding significance for protecting the environment and saving resources.

INDEX TERMS Tangentially fired furnace, super-resolution reconstruction,smoke black concentration field,three-dimensional reconstruction.

I. INTRODUCTION

The tangentially fired furnace has the advantages of sufficient combustion and low NOx emissions. Four of the air streams form an imaginary circle in the center of the furnace. This tangential combustion method can make the air streams emitted by adjacent burners ignite each other, and help the air stream ignite. To better control the combustion situation in the furnace, it is of great significance to monitor the flame field and smoke black concentration field in the furnace.

When the method of computer vision used to analyze the flame field in the furnace, due to the low resolution of the industrial camera and the smoke generated by the flame combustion, the image inside the flame field obtained has low resolution and poor image quality, which brings great difficulties to the related research of the furnace flame field. To obtain more accurate research results on the furnace flame field, the most important thing is to improve the resolution of the furnace flame image.

The learning-based method is a hot topic in the research of super-resolution algorithms in recent years. It uses a large number of high-resolution image construction learning libraries to generate learning models. It introduces the priors obtained by the learning models in the process of restoring low-resolution images. Knowledge to get high-frequency details of the image and get better image restoration results. Ledig *et al.* [1] proposed SRGAN. This method is the first to use a generative adversarial network to solve the problem of super-resolution. The recovered image usually loses high-frequency information, thereby reducing the visual perception. Wang *et al.* [2] proposed an enhanced ESRGAN network model. This algorithm is suitable for images with

The associate editor coordinating the review of this manuscript and approving it for publication was Hengyong Yu.

more feature details. The flame images captured in the industrial environment are not suitable for reconstruction with this super-resolution method due to their large noise, lack of luxurious features,and unclear texture. Jiang *et al.* [3] proposed an image enhancement algorithm based on GAN for satellite images, which can learn the texture and detail edge of the image simultaneously by constructing two subnets. Gazzola *et al.* [4] proposed a new internal and external iterative algorithm for edge enhancement in imaging problems. By using the adaptive diagonal weighting matrix to design regularization operators, smoothness was enhanced effectively. Wang *et al.* [5] proposed a GAN-based remote sensing image SR reconstruction technology. They proposed a two-dimensional ultra-high-density residual block (UDRB) for feature extraction and fusion to train more realistic reconstruction results. Zhang *et al.* [6] proposed a deep residual channel attention network to make the network focus on learning high-frequency information. Yi *et al.* [7] proposed a multi-time ultra-dense memory (MTUDM) network for video super-resolution. They designed an ultra-high density memory block (UDMB) to make full use of intra-frame spatial correlation and inter-frame temporal correlation, to recover more real image details. Wang *et al.* [8] proposed a video super-resolution multi-memory network, integrating different modules to make full use of spatial correlation within frames and temporal between frames. Jiang *et al.* [9] combined multiple deep learning models and proposed a multi-model fusion network (ATMFN) based on the adaptive threshold to solve the compressed face illusion problem. Jiang *et al.* [10] proposed a multi-path UDB for local feature extraction and fusion based on remote sensing images, it promoted feature expression by advocating a rectification and compensation mechanism. Chen *et al.* [11] has proposed the single-image SR algorithm based on structural self-similarity and deformation block features.

Based on the flame characteristics of the tangentially fired furnace, this article proposes a strengthened edge characteristic super-resolution network (SECSR) suitable for furnace flame images. This method can better detect the edge of the flame, strengthen the characteristics of the flame edge, and contribute to the super-resolution reconstruction of the flame image.

Based on the results of this research, this article proposes a new three-dimensional reconstruction method of the furnace flame soot concentration field.

The measurement method of smoke black concentration is mainly non-contact measurement, which will not destroy the smoke black concentration field in the furnace, ensure the accuracy of the measurement, and eliminate the artificial interference of the contact measurement on the object measurement.

Ayranci *et al.* [12], [13] used flame images and flame tomography to simultaneously reconstruct the flame temperature field and the smoke black concentration field. His method was only suitable for symmetrical flames, not for asymmetric flames of a tangential burner.

Qamar *et al.* [14] used laser-induced incandescence to measure the soot volume fraction in three different turbulent diffusion flames. When the laser irradiates the smoke, the smoke particles rapidly heat up due to absorbed energy and emit black body radiation corresponding to the increased temperature. The quantitative distribution of smoke concentration is obtained by measuring the laser light intensity signal of the smoke particles after excitation and combining the calibration method. This method is affected by the laser irradiation range and the degree of laser attenuation, and only reflect the smoke and blackness in local areas.

Wei [15] team proposed a three-dimensional reconstruction method of furnace flame temperature field based on radiation inversion. This method performs longitudinal inversion calculation based on the synchronized flame images collected at different wavelengths, reconstruct the three-dimensional reconstruction of the furnace flame temperature field. Based on the research results of this team, this article proposes a new three-dimensional reconstruction method of flame smoke black concentration field in a tangentially fired furnace.

For this article, the main contributions are as follows:

(1) This article proposes a strengthen edge characteristic super-resolution network (SECSR) algorithm suitable for the tangentially fired furnace flame images. This algorithm effectively improves the quality of the furnace flame image, reduces the edge jagged, and provides high-quality flame images for the study of the furnace flame field.

(2) Based on the super-resolution reconstruction of the flame image, this article proposes an inversion algorithm for the smoke density field of the tangentially fired furnace. The high-precision tangentially fired furnace flame temperature field is obtained through inversion calculation to calculate the soot concentration field, which has better control of the fuel combustion in the furnace.

II. SUPER-RESOLUTION RECONSTRUCTION ALGORITHM AND THREE-DIMENSIONAL RECONSTRUCTION METHOD OF SMOKE BLACK CONCENTRATION FIELD

A. SUPER-RESOLUTION RECONSTRUCTION ALGORITHM OF FLAME IMAGE IN A TANGENTIALLY FIRED FURNACE

The GAN network adds an adversarial model to the generative model and forms an adversarial mechanism. Various variants based on GAN networks have been widely used in image processing. The SRGAN network applies GAN to image super-resolution. The GAN network trains a generator to generate realistic samples from random noise and trains a discriminator to discriminate generated data from real data. When the training reaches a balance, the discriminator can not distinguish between real and generated samples. In terms of image super-resolution, GAN networks can generate high-quality image samples, reconstruct realistic image textures and high-quality images. The image features of the flame are not rich enough and the texture is not clear enough. Due to the smoke produced by insufficient flame combustion [16], [17], the edges of the image are jagged severely. It is

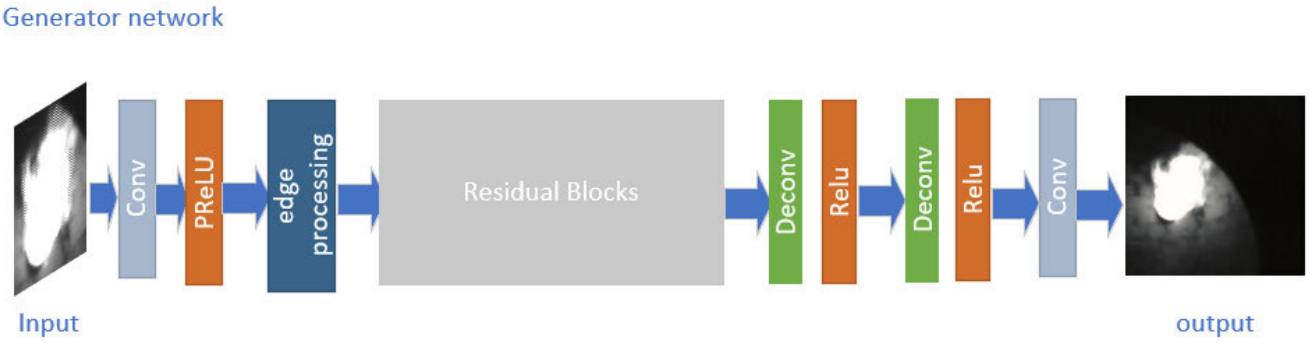

FIGURE 1. Generator network structure diagram on the flame image reconstruction.

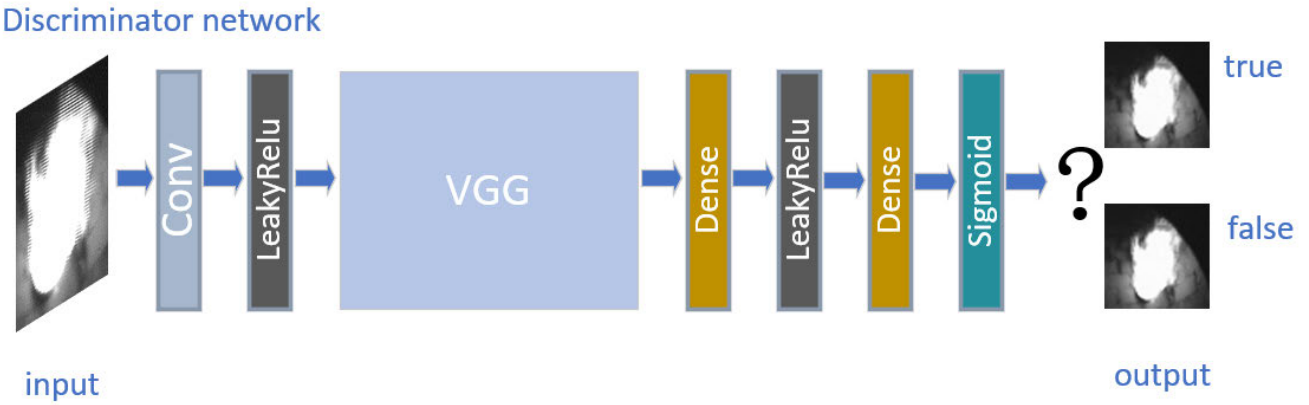

FIGURE 2. Discriminator network structure diagram on flame image reconstruction.

difficult for the network to learn a large number of features for reconstruction. Based on the SRGAN network, this article proposes a super-resolution reconstruction network suitable for the flame image of a tangential furnace.

1) NETWORK STRUCTURE

The algorithm based on the GAN network framework and aims to improve the quality of flame images. The network structure consists of a generator and a discriminator, as shown in Fig.1 and Fig.2. The generator network is composed of an edge processing module, residual block, and convolutional layer. The discriminator network is composed of VGG network, LeakyRelu, convolutional layer, sigmoid. The input low-resolution image I^{LR} obtains the super-resolution image I^{SR} through the generator network, the discriminator network continuously learns the image features through training to distinguish the generated image I^{SR} and the real natural image I^{HR}.

The generator and the discriminator are trained to reach a balance, which the discriminator cannot distinguish whether the input image is a generated image or a real natural image. The generator network and the discriminator network are optimized alternately to solve the minimum-maximum problem, to achieve the purpose of image super-resolution.

$$\min_{\theta_G}\max_{\theta_D} E_I^{\mathrm{HR}} \sim \mathrm{ptrain}\left(\mathrm{I}^{\mathrm{HR}}\right)\left[\log \mathrm{D}_\theta\left(\mathrm{I}^{\mathrm{HR}}\right)\right] + \mathrm{E}_{\mathrm{I}}^{\mathrm{LR}} \sim \mathrm{p}G\left(I^{LR}\right)\left[\log\left(1 - D_{\theta D}\left(G_{\theta G}\left(I^{LR}\right)\right)\right)\right] \quad (1)$$

2) EDGE PROCESSING MODULE

To solve the problem of fuzzy edges of the flame images, this article adds an edge processing module to the generator network. Firstly, the edge of the flame image is detected. Edge points refer to the pixel points in the image whose local brightness changes significantly. Since the collected image features are single and the contour is simple, the Sobel operator is used to calculate the image with simple and fast speed [18], [19], so the edge detection effect of a simple contour image is good and clear contour can be obtained.

The convolution template used by the Sobel operator is:

$$G_{\mathrm{x}} = \begin{bmatrix} -1 & 0 & 1 \\ -2 & 0 & 2 \\ -1 & 0 & 1 \end{bmatrix} \quad G_y = \begin{bmatrix} -1 & -2 & -1 \\ 0 & 0 & 0 \\ 1 & 2 & 1 \end{bmatrix}$$

After edge detection, 8∗8 neighborhood pixels are obtained at each pixel point on the edge of the gray image, because

the gray difference around the edge of the image is large.The K-means algorithm is used to classify the neighborhood pixel values. The clustering method is used to process the neighborhood pixel values of the edge points, and the neighborhood pixel values are divided into three categories, which respectively represent the internal flame pixel value, the flame edge pixel value, and the image background pixel value. After obtaining the pixel value of the classified cluster center, E_1, E_2, E_3 represent the values of the three cluster centers respectively, average $=$ (E1 $+$ E2 $+$ E3), and the value of average is assigned to the edge pixel points, to reduce the gray value difference of edge pixel points and thus reduce the sawtooth.

In the generator network, through the edge processing module, the network will learn a lot of edge features of the furnace flame image.The edge-enhanced feature map is input into the residual network to continue learning, which can effectively extract the features of the image to strengthen the overall learning ability of the network. It helps the generator network to realize the super-resolution reconstruction and improve image quality.

3) RESIDUAL NETWORK

In this article, the residual block network in the generator network is used to solve the gradient explosion or disappearance, convergence difficulty, performance degradation, and other problems caused by the deep convolutional network. The residual structure is shown in Fig.3.

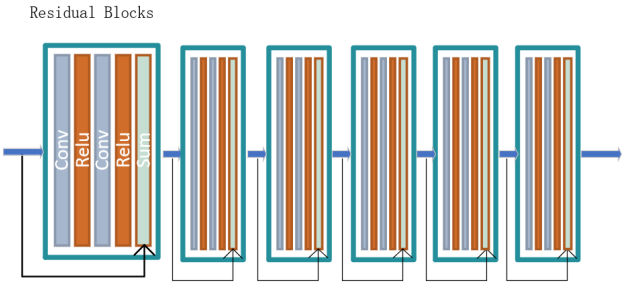

FIGURE 3. The network structure of the residual block.

Each residual block is composed of a convolutional layer and a Relu activation function. The input feature map is processed by the edge processing module to extract the edge of the flame image effectively. We use two $3 * 3$ convolution kernels to process the merged feature map, reducing the number of feature maps to 64. The purpose is to release parameters and computational complexity, extract more concise information, and use the Relu activation function.

4) LOSS FUNCTION

The algorithm loss function proposed consists of two parts: generator network loss function and discriminator network loss function.

The generator network loss function is defined as:

$$l^{SR}_{VGG/i,j} = \frac{1}{W_{i,j}H_{i,j}} \sum_{x=1}^{W_{i,j}} \sum_{y=1}^{H_{i,j}} \left(\phi_{i,j}\left(I^{HR}\right)_{x,y} - \phi_{i,j}\left(G_{\theta 6}\left(I^{LR}\right)\right)_{x,y} \right)^2 \tag{2}$$

When training the network, using the mean square error loss can obtain a higher peak signal-to-noise ratio, but the restored image will lose a lot of high-frequency details. This article input the generated image and the target image into the VGG network separately, and then calculate the Euclidean distance from the feature map obtained after passing through the VGG, and use it as the VGG loss. $\phi_{i,j}$ represents the feature map obtained by the j-th convolution before the i-th largest pooling layer in the VGG network,$W_{i,j}$ and $H_{i,j}$ are the sizes of the feature maps of the VGG network.

The discriminator network loss function is defined as:

$$l^{SR}_{Gen} = \sum_{n=1}^{N} \left(-\log D_{\theta D}\left(G_{\theta 6}\left(I^{LR}\right)\right)\right) \tag{3}$$

Among them, $D_{\theta D}\left(G_{\theta G}\left(I^{LR}\right)\right)$ is the probability that the generated image $G_{\theta_G}\left(I^{LR}\right)$ is a real natural image.

The overall workflow of the super-resolution reconstruction algorithm is as follows:

Step 1: Clipping the image in the data set, the image size is $256 * 256$ and the image format is PNG.

Step 2: In the edge detection module, set the neighborhood of each pixel selected as $8 * 8$, and set $K = 3$ for K-means algorithm.

Step 3: Training network. The experiment uses the images in the training set as the input of the network. For optimization, we use Adam with $\beta_1 = 0.9, \beta_2 = 0.999$. We alternately update the generator and discriminator network until the model converges. The learning rate is initialized as 10^{-4} and decayed by a factor of 2 every $2 * 10^5$ of mini-batch updates.

Step 3.1: Training the SRResnet network to get the original generator network. The input is the low score I^{LR} image after I^{HR} downsampling, and the output is the super score picture I^{SR} generated after reconstruction of the low score I^{LR}.

Step 3.2: The experiment retains all the parameters of the generator network and initializes the discriminator network parameters randomly to train the SECSR network.

Step 3.3: The experiment retains all the parameters of the network and introduces the VGG network. The VGG network is used to extract the features of the real picture I^{HR} and the generated picture I^{SR}, and the difference between the two features is calculated as a loss function to better retain the image detail information.

Step 4: The article uses the optimal network model to reconstruct the flame image.

B. INVERSION METHOD OF SMOKE BLACK CONCENTRATION IN A TANGENTIALLY FIRED FURNACE

The theoretical value of thermal radiation is based on the black body radiation law. The Black body refers to the complete absorption of external radiation under any conditions and the conversion of these radiations into thermal radiation. Its spectral characteristics have nothing to do with the material, but only with the temperature of the object.

The Planck radiation formula gives a calculation of the amount of blackbody radiation at a specific wavelength and temperature. The calculation is as follows:

$$I_b(\lambda, T) = \frac{C_1}{\lambda^5}\left[\exp\left(\frac{C_2}{\lambda T}\right) - 1\right]^{-1} \tag{4}$$

$I_b(\lambda, T)$ is the radiation intensity of the black body from a radiation plane to the whole hemisphere at a wavelength of λ,the unit is $W/\left(m^2 \cdot \mu m\right)$;$C_1$ is the first Planck radiation constant $C_1 = 3.743 \times 108 \quad W \cdot \mu m^2$;$C_2$ is the second Planck radiation constant $C_2 = 1.439 \times 104 \mu m \cdot K$;λ is the wavelength, and T is the absolute temperature of the black body.

The flame is not a black body, so its absorption rate is not 1. Based on the black body, the formula for redefining the radiation of a flame is:

$$I(\lambda, T) = \varepsilon(\lambda, T) \cdot I_b(\lambda, T) \tag{5}$$

When the wavelength is 300-1000 nm, the temperature is 600k-2000k, and C2/λT $\gg$ 1, Planck's law can be replaced by Wayne's law. At this time, the formula for calculating the radiant energy of the flame is as follows:

$$I(\lambda, T) = \varepsilon(\lambda, T) \cdot \frac{C_1}{\pi\lambda^5}\exp\left(-\frac{C_2}{\lambda T}\right) \tag{6}$$

$$\varepsilon(\lambda, T) = 1 - \exp\left(\frac{-K_{abs} l}{\lambda^\beta}\right) \tag{7}$$

$K_{abs} = 6\pi E(m) f_v/\lambda, f_v$ is the smoke black concentration, and E(m) is constant at a specific wavelength,so K_{abs} is proportional to smoke black concentration f_v,l indicates the flame thickness of the detection system along the optical axis. Parameter β is related to the physical and optical characteristics of smoke black.

The image acquisition system synchronously obtains the flame image in multiple wavebands from four angles. Now only the radiant energy of the flame image in a certain wavelength in the same direction is considered. The gray value of each pixel in the flame image is related to the radiant energy of a ray obtained from the CCD [20] camera surface. The radiant energy represented by the pixel value is calculated as follows:

$$E(\lambda_k, T) = K_\lambda \cdot G \tag{8}$$

K_λ is the wavelength λ, the linear correlation gain coefficient between the monochromatic radiation intensity and the gray value of the temperature T. G is the gray value of the pixel. The radiant intensity at a point in a grayscale image is equal to the sum of the radiant energy values of a ray along the longitudinal direction, and the accumulation of radiant energy on this ray can be expressed by the following formula:

$$E(\lambda_k, T) = \int_0^{S_f} I(\lambda_k, T)\, ds = \int_0^{S_f} \varepsilon(\lambda_k, T) \cdot I_b(\lambda_k, T)\, ds \tag{9}$$

In the formula,S_f indicates the flame radiation formula. $\varepsilon(\lambda_k, T)$ represents the flame radiation monochromatic emissivity, $I_b(\lambda_k, T)$ represents the black body radiation value at a wavelength of λ_k and a temperature of T.

The integral calculation is not easy to solve by computer. This ray is reduced to n segments. This ray is divided into m pixels in m pictures after being split by a spectrometer. The radiation value of each segment can be given according to (10) so that the integral in (9) can be converted into the superposition of n radiation fields. (9) can be rewritten as follows:

$$\begin{aligned} E(\lambda_k, T) &= \int_0^{S_f} \varepsilon(\lambda_k, T) \cdot I_b(\lambda_k, T)\, ds \\ &= \sum_{i=1}^{n} \varepsilon(\lambda_k, T_i) \cdot I_b(\lambda_k, T_i)\, l(i) \end{aligned} \tag{10}$$

$l(i)$ indicates the length of the i-th segment in the ray. For other parameters, refer to (9). Substituting the parameters in (12) gives (11):

$$\begin{aligned} &E(\lambda_k, T) \\ &= \sum_{i=1}^{n} \frac{36\pi nk}{\left(n^2 - k^2 + 2\right)^2 + 4n^2k^2}\frac{f_v(i)}{\lambda_k} \cdot I_b(\lambda_k, T_i)\, l(i) \end{aligned} \tag{11}$$

There are 2n unknowns in (11), which cannot be solved directly. (11) is only the formula of λ_k in a certain band, and the synchronization pictures of m bands are obtained. According to (10), the following equation group:

$$\begin{cases} E(\lambda_1, T) = \sum_{i=1}^{n} \varepsilon(\lambda_1, T_i) \cdot I_b(\lambda_1, T_i)\, l(i) \\ E(\lambda_2, T) = \sum_{i=1}^{n} \varepsilon(\lambda_2, T_i) \cdot I_b(\lambda_2, T_i)\, l(i) \\ \cdots \\ E(\lambda_m, T) = \sum_{i=1}^{n} \varepsilon(\lambda_m, T_i) \cdot I_b(\lambda_m, T_i)\, l(i) \end{cases} \tag{12}$$

By solving the above equations, we can get the smoke concentration value of n segment of a certain ray, and address each pixel point in the image. Three-dimensional reconstruction of the smoke concentration field can be carried out in one direction to get the situation of all smoke concentration fields in the furnace.

Assuming that the size of the image obtained after super-resolution reconstruction is h*w and the number of segments obtained by longitudinal inversion calculation is n,

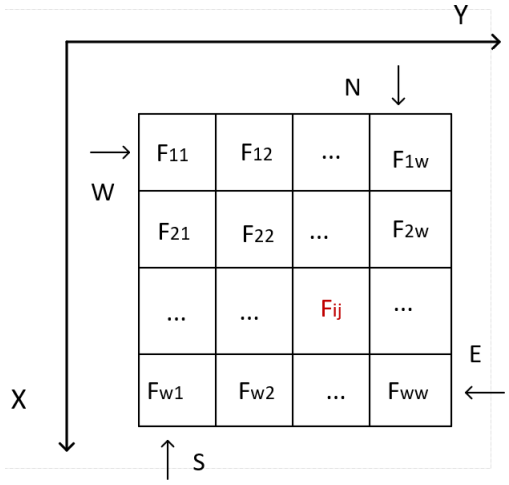

FIGURE 4. The calculation process of the fusion of smoke and black at the same level.

the furnace chamber is divided into an h*w*n region in one direction. In fact, w is much larger than n. To facilitate superposition calculation, the n segment obtained by inversion calculation is extended to w segment by linear interpolation method, and an h*w*w precision smoke black concentration field is obtained in the one-way direction. Since the camera is at a horizontal height, the fusion algorithm has nothing to do with the height. Firstly, the fusion algorithm at a certain height is analyzed.

The coordinate graph of the fusion calculation is given below. The fusion direction is based on the camera in the south direction.

For each direction, the upper left corner is the origin of the coordinates, and S, N, W, and E are the smoke concentration fields reflected from the south, north, west, and east respectively. F represents the smoke black concentration field obtained by fusion calculation. The reference coordinate directions of F and S are the same. The formula for calculating F based on S, N, W, E is shown below:

$$F(i,j) = \frac{1}{4}(S(i,j) + N(w-i,w-j) + w(w-i,j) + E(i,w-j)) \quad (13)$$

w represents the width of the image after super-resolution reconstruction. According to (13), the exact smoke concentration value at a certain height can be calculated, and then the same calculation can be done for any height. In this way, an accurate h * w * w three-dimensional smoke black concentration field can be obtained. The calculation methods are all completed.

III. EXPERIMENT AND ANALYSIS OF RESULTS

A. EXPERIMENT APPARATUS

Fig.5 is a flame image acquisition system for a tangentially fired furnace. The system structure is shown below.

Fig.5 (a) is a reduced version of a four-corner round furnace. To reduce the complexity of combustion, only one layer

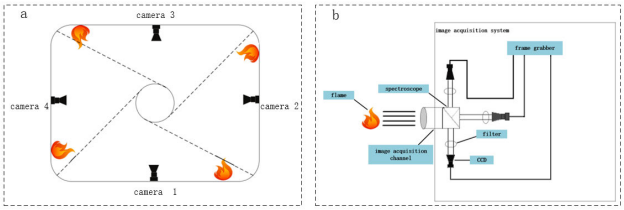

FIGURE 5. Image acquisition system of flame in tangentially fired furnace.

of burners is deployed, which are distributed in the four corners of the furnace. The burner is connected to the oil pipeline and the ventilation pipe. There are observation holes. Through these four observation ports, CCD cameras can be deployed to take pictures. There are thermocouple insertion holes on the east and west sides.Fig.5(a) is the model view of the furnace,an image acquisition system is arranged around as shown in Fig. 5(b). The flame light is divided into three synchronous beams by a beam splitting device. There is a filtering device between the CCD camera and the beam splitting device.The three wavelengths retained in the experiment are 550nm, 600nm, and 635nm.Using the calibration-free wavelength modulation spectroscopy technology proposed by Guo *et al.* [21] can reduce the impact of environmental common mode noise. Because image acquisition devices are arranged around the furnace, 12 sets of synchronously filtered flame pictures in four directions can be obtained at the same time. The combustion equipment and images are given below.The following is a physical picture of the combustion equipment and image acquisition equipment:

The silver large-caliber tube in the burner section in Fig.6 provides hot air for the furnace, and the thin tube provides diesel. Therefore, the fuel inside the furnace is a mixture of air and diesel. The initial fuel to air ratio is 1 to 15. The air velocity is about 5m/s, and the fuel flow rate is about

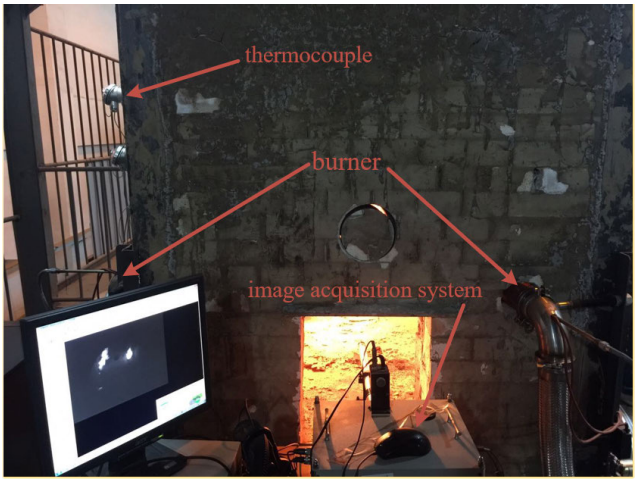

FIGURE 6. Tangentially fired furnace in the experiment.

TABLE 1. Image quality results of different super-resolution algorithms.

Algorithms	set5	set14	B100	Urban100
	PSNR/SSIM/NIQE/PI	PSNR/SSIM/NIQE/PI	PSNR/SSIM/NIQE/PI	PSNR/SSIM/NIQE/PI
Original	29.01/0.74/5.32/5.17	28.37/0.59/5.64/5.36	28.12/0.62/5.15/6.88	27.98/0.68/6.18/5.68
Bicubic interpolation	30.27/0.82/5.98/6.31	27.56/0.76/5.88/4.86	29.87/0.71/5.46/6.15	27.55/0.75/6.34/5.33
SRGAN algorithms	31.45/0.86/6.31/5.82	29.23/0.84/6.13/5.57	29.45/0.77/6.35/5.66	28.34/0.79/6.94/4.75
SECSR algorithms	32.14/0.91/6.75/3.21	30.12/0.89/6.54/4.08	30.32/0.85/6.81/4.37	28.75/0.81/7.15/3.83

0.0012kg/s. This ratio will be adjusted based on the predicted value of the smoke black concentration in the future.

B. SUPER-RESOLUTION RECONSTRUCTION EXPERIMENT OF FLAME IMAGE IN A TANGENTIAL FURNACE

1) EXPERIMENTAL DETAILS

The training data set for this experiment consists of two parts. The first part is 6000 high-definition images in the ImageNet data set, and the second part comes from the furnace flame images and about 1000 high-definition flame images. The validation data set includes Set5, Set14, B100 and Urban100 data sets.

The experiment uses the images in the training set as the input of the network. For optimization, we use Adam with $\beta_1 = 0.9$, $\beta_2 = 0.999$. We alternately update the generator and discriminator network until the model converges.The learning rate is initialized as 10^{-4} and decayed by a factor of 2 every $2 * 10^5$ of mini-batch updates. We implement our models with the Tensorflow framework and train them using NVIDIA GeForce RTX 2080 Ti GPUs.

2) EXPERIMENTAL RESULTS AND ANALYSIS

After the training of the flame image reconstruction network proposed in Section 2.1, the optimal model is selected for testing, and the super-reconstructed image visual effect is obtained.Fig.7 (a) is the image before super-resolution reconstruction, Fig.7(b) is the image after super-resolution reconstruction, and the image in the lower right corner is the enlarged detail of the red area. The experimental results are shown in Fig.7.

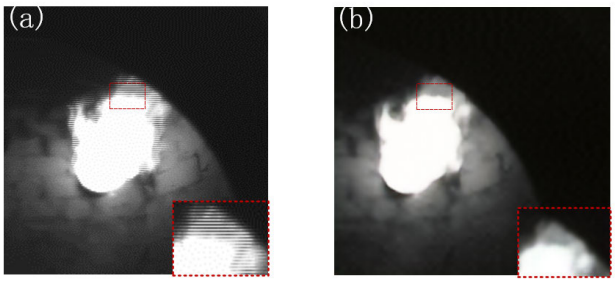

FIGURE 7. Experimental results of super-resolution reconstruction.

The results after super-resolution reconstruction are compared with the bicubic interpolation algorithm and SRGAN algorithm, and the results are shown in Fig.8.

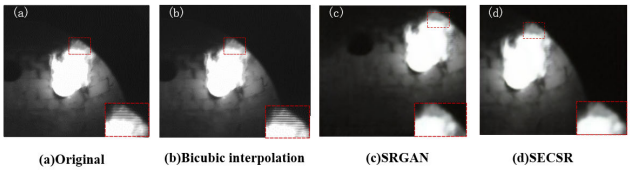

FIGURE 8. Subjective comparison of super-resolution results of flame images processed by different algorithms.

To verify the effectiveness of the algorithm, this article verifies the three algorithms on the Set5, Set14, B100 and Urban100 data sets, using PSNR, SSIM, NIQE [22] and PI indicators to calculate image quality. The results are shown in Table 1.

From the data in Table 1, after super-resolution reconstruction using the algorithm proposed in this article, the jagged condition of the flame image edge has been greatly improved, the artifacts are reduced, the details of the image edge are more abundant, and the image quality has been greatly improved. Improved, the image can meet the requirements of three-dimensional soot concentration field reconstruction.

C. RECONSTRUCTION EXPERIMENT OF SMOKE BLACK CONCENTRATION FIELD IN A TANGENTIALLY FIRED FURNACE

1) DATA SIMULATION EXPERIMENT

Fig.9 is a synchronized picture of 12 flames taken in four directions at a certain moment, as shown below:

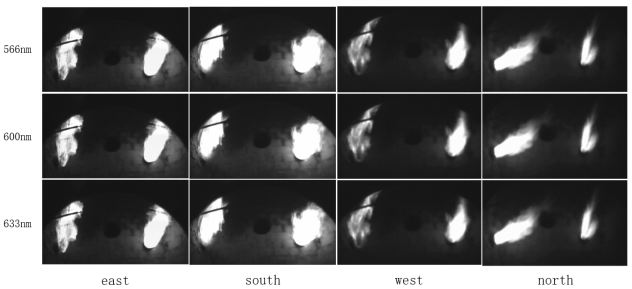

FIGURE 9. Synchronized filtered image.

The three-dimensional reconstruction of the smoke black concentration field in the furnace according to the picture in Fig.9 and the theoretical knowledge. Fig.10 shows the smoke black concentration in the furnace at a certain time, and Fig.11 shows the smoke black concentration distribution in the z-axis direction. The three-dimensional smoke black

TABLE 2. Comparison of 1/4 height thermocouple acquisition point and inverse calculation of smoke black concentration.

Collection point	A1	A2	A3	A4	A5	A6	A7	A8	A9
Inversion calculation(ppm)	2.37	4.76	1.28	2.13	2.84	2.34	3.24	4.73	1.24
thermocouple(ppm)	2.43	4.69	1.25	2.12	2.78	2.37	3.34	4.69	1.21
Average error(%)	2.8	1.4	2.4	0.4	1.7	1.6	2.9	0.8	2.4

TABLE 3. Comparison of 1/2 height thermocouple acquisition point and inverse calculation of smoke black concentration.

Collection point	B1	B2	B3	B4	B5	B6	B7	B8	B9
Inversion calculation(ppm)	1.67	3.86	1.38	1.69	2.64	2.22	3.01	4.68	1.23
thermocouple(ppm)	1.63	3.89	1.36	2.12	2.63	2.27	3.04	4.69	1.22
Average error(%)	2.4	0.7	1.4	0.4	0.3	1.7	1.0	0.2	0.8

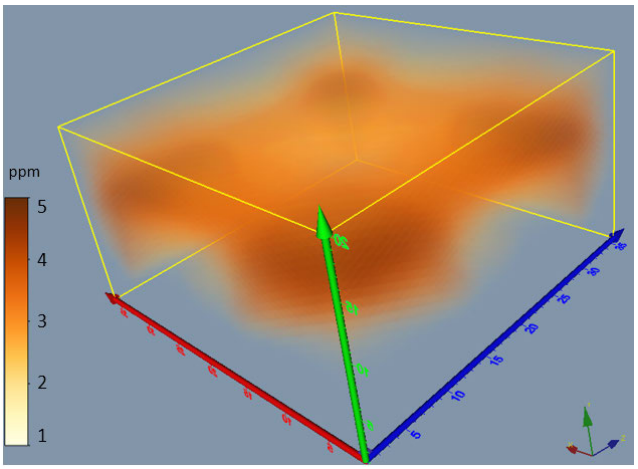

FIGURE 10. Three-dimensional smoke concentration field in furnace.

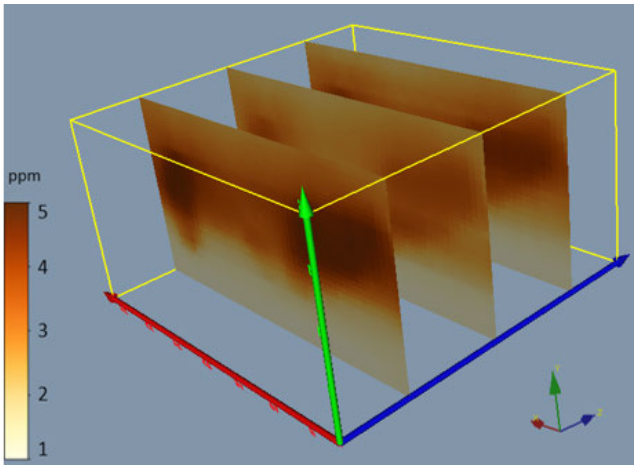

FIGURE 11. Smoke black concentration field cutaway.

concentration field calculated by the inversion is in accordance with the theory of thermodynamics and the combustion conditions in a tangential burner. After the inversion calculation, the real-time smoke black concentration can be calculated, and the combustion in the furnace can be better controlled.

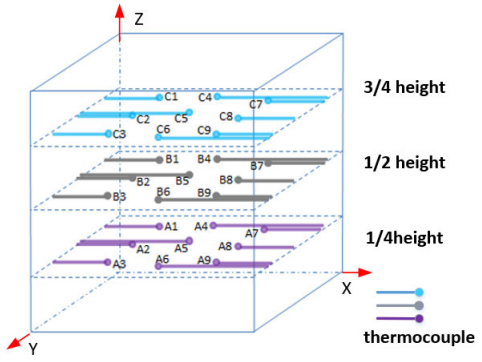

FIGURE 12. Thermocouple distribution.

According to the comparison of the actual flame burning situation and the theoretical basis of smoke black concentration, the three-dimensional effect map and the smoke black concentration field section view are in line with expectations, so it can be initially determined that the method based on radiation inversion calculation of smoke black concentration is effective.

2) COMPARATIVE EXPERIMENTAL VERIFICATION

To further verify the validity of the flame smoke black concentration inversion method, a comparison was made between the smoke black concentration calculated by the inversion and the thermocouple particle density method.

Fig.12 is the distribution diagram of the thermocouple of the tangentially fired furnace. The location of the thermocouple is consistent with the plane of the cross section of the smoke black concentration field of Fig. 9, where A1 $\sim$ A9, B1 $\sim$ B9, and C1 $\sim$ C9 respectively represent 1/4, 1/2, 3/4 height thermocouples.The smoke black concentration calculated by the thermocouple and inversion in the experimental stage is shown below:

According to Table 2, it is calculated that the error of the smoke black concentration at the 1/4 height thermocouple acquisition point and the inversion calculation is about 1.8%.

According to Table 3, it is calculated that the error of the smoke black concentration at the 1/2 height thermocouple acquisition point and the inversion calculation is about 0.98%.

TABLE 4. Comparison of 3/4 height thermocouple acquisition point and inverse calculation of smoke black concentration.

Collection point	C1	C2	C3	C4	C5	C6	C7	C8	C9
Inversion calculation(ppm)	2.12	4.36	1.41	2.24	3.04	2.35	3.72	4.57	1.33
thermocouple(ppm)	2.07	4.39	1.39	2.22	2.98	2.38	3.77	4.7	1.31
Average error(%)	2.4	0.6	1.4	0.9	2.0	1.2	1.3	2.7	1.5

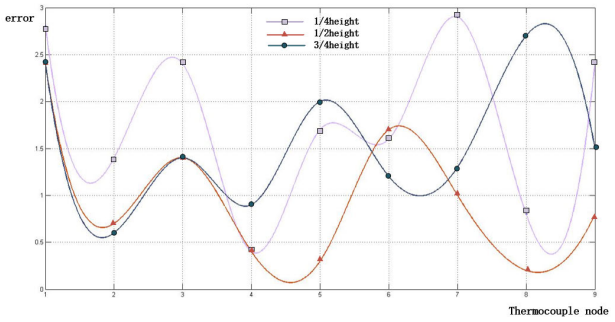

FIGURE 13. Distribution of measurement errors at different height nodes.

According to Table 4, it is calculated that the error of the smoke black concentration at the 3/4 height thermocouple acquisition point and the inversion calculation is about 1.4%.

Fig.13 shows the error situation at three altitudes. Based on all the data, the weighted average error of the smoke black concentration measurement method proposed in this article is about 1.3%, it can effectively verify the smoke black concentration measurement method based on radiation inversion.It is worth noting that, compared with the contact thermocouple measurement method, the radiation inversion is better in real-time and the measurement is more accurate.

IV. CONCLUSION

Summarizing the characteristics of the current mainstream algorithms, they are not suitable for the super-resolution reconstruction of furnace flame images. This article proposes an enhanced edge feature super-resolution reconstruction algorithm suitable for tangentially fired furnace flame image.According to the calculation of different image evaluation indicators, the algorithm proposed in this article can reduce the jagged edge of the image and influence of noise, and obtain high-resolution tangentially fired furnace flame image.Compared with the measurement results of the thermocouple method, the inversion method proposed in this article has a weighted average error of about 1.3%, and the inversion method can obtain high-precision tangentially circular furnace soot concentration field.Experimental results show that the super-resolution reconstruction algorithm proposed in this article can significantly improve the calculation accuracy of the flame temperature field in the furnace. Thus, the accurate smoke black concentration field in the furnace can be obtained through inversion calculation, and the combustion situation of fuel in the furnace can be better understood.

REFERENCES

[1] C. Ledig, L. Theis, F. Huszar, J. Caballero, A. Cunningham, A. Acosta, A. Aitken, A. Tejani, J. Totz, Z. Wang, and W. Shi, "Photo-realistic single image super-resolution using a generative adversarial network," in *Proc. IEEE Conf. Comput. Vis. Pattern Recognit. (CVPR)*, Jul. 2017, pp. 105–114.

[2] N. C. Rakotonirina and A. Rasoanaivo, "ESRGAN+: Further improving enhanced super-resolution generative adversarial network," in *Proc. IEEE Int. Conf. Acoust., Speech Signal Process. (ICASSP)*, May 2020, pp. 63–79.

[3] K. Jiang, Z. Wang, P. Yi, G. Wang, T. Lu, and J. Jiang, "Edge-enhanced GAN for remote sensing image superresolution," *IEEE Trans. Geosci. Remote Sens.*, vol. 57, no. 8, pp. 5799–5812, Aug. 2019.

[4] S. Gazzola, M. E. Kilmer, J. G. Nagy, O. Semerici, and E. L. Miller, "An inner-outer iterative method for edge preservation in image restoration and reconstruction," Tech. Rep., 2019.

[5] Z. Wang, K. Jiang, P. Yi, Z. Han, and Z. He, "Ultra-dense GAN for satellite imagery super-resolution," *Neurocomputing*, vol. 398, pp. 328–337, Jul. 2020. [Online]. Available: http://www.sciencedirect.com/science/article/pii/S0925231219314602

[6] Y. Zhang, K. Li, K. Li, L. Wang, B. Zhong, and Y. Fu, "Image super-resolution using very deep residual channel attention networks," Tech. Rep., 2018.

[7] P. Yi, Z. Wang, K. Jiang, Z. Shao, and J. Ma, "Multi-temporal ultra dense memory network for video super-resolution," *IEEE Trans. Circuits Syst. Video Technol.*, vol. 30, no. 8, pp. 2503–2516, Aug. 2020.

[8] Z. Wang, P. Yi, K. Jiang, J. Jiang, Z. Han, T. Lu, and J. Ma, "Multi-memory convolutional neural network for video super-resolution," *IEEE Trans. Image Process.*, vol. 28, no. 5, pp. 2530–2544, May 2019.

[9] K. Jiang, Z. Wang, P. Yi, G. Wang, K. Gu, and J. Jiang, "ATMFN: Adaptive-threshold-based multi-model fusion network for compressed face Hallucination," *IEEE Trans. Multimedia*, early access, Dec. 18, 2020, doi: 10.1109/TMM.2019.2960586.

[10] K. Jiang, Z. Wang, P. Yi, J. Jiang, J. Xiao, and Y. Yao, "Deep distillation recursive network for remote sensing imagery super-resolution," *Remote Sens.*, vol. 10, no. 11, p. 1700, Oct. 2018.

[11] Y. Chen, J. Wang, X. Chen, M. Zhu, and R. Xia, "Single-image super-resolution algorithm based on structural self-similarity and deformation block features," *IEEE Access*, vol. 7, pp. 58791–58801, 2019.

[12] I. Ayrancá, R. Vaillon, N. Selçuk, F. André, and D. Escudié, "Determination of soot temperature, volume fraction and refractive index from flame emission spectrometry," *J. Quant. Spectrosc. Radiat. Transf.*, vol. 104, no. 2, pp. 266–276, Mar. 2007.

[13] I. Ayrancá, R. Vaillon, and N. Selçuk, "Near-infrared emission spectrometry measurements for nonintrusive soot diagnostics in flames," *J. Quant. Spectrosc. Radiat. Transf.*, vol. 109, no. 2, pp. 349–361, Jan. 2008.

[14] N. H. Qamar, G. J. Nathan, Z. T. Alwahabi, and K. D. King, "The effect of global mixing on soot volume fraction: Measurements in simple jet, precessing jet, and bluff body flames," *Proc. Combustion Inst.*, vol. 30, no. 1, pp. 1493–1500, Jan. 2005.

[15] Z. Wei, H. Ge, L. Wang, and Z. Li, "3-D temperature reconstruction of the flame field in a tangentially fired furnace," *IEEE Trans. Instrum. Meas.*, vol. 67, no. 8, pp. 1929–1939, Aug. 2018.

[16] Q.-X. Huang, F. Wang, D. Liu, Z.-Y. Ma, J.-H. Yan, Y. Chi, and K.-F. Cen, "Reconstruction of soot temperature and volume fraction profiles of an asymmetric flame using stereoscopic tomography," *Combustion Flame*, vol. 156, no. 3, pp. 565–573, Mar. 2009. [Online]. Available: http://www.sciencedirect.com/science/article/pii/S0010218009000029

[17] Q. Huang, F. Wang, J. Yan, and Y. Chi, "Simultaneous estimation of the 3-D soot temperature and volume fraction distributions in asymmetric flames using high-speed stereoscopic images," *Appl. Opt.*, vol. 51, no. 15, p. 2968, 2012.

[18] Z. Xiangxi, Z. Yonghui, Z. Shuaiyan, and Z. Jian, "FPGA implementation of edge detection for sobel operator in eight directions," in *Proc. IEEE Asia Pacific Conf. Circuits Syst. (APCCAS)*, Oct. 2018, pp. 520–523.

[19] K. Zhang, Y. Zhang, P. Wang, Y. Tian, and J. Yang, "An improved sobel edge algorithm and FPGA implementation," *Procedia Comput. Sci.*, vol. 131, pp. 243–248, Dec. 2018. [Online]. Available: http://www.sciencedirect.com/science/article/pii/S1877050918305891
[20] C. Lou, H.-C. Zhou, P.-F. Yu, and Z.-W. Jiang, "Measurements of the flame emissivity and radiative properties of particulate medium in pulverized-coal-fired boiler furnaces by image processing of visible radiation," *Proc. Combustion Inst.*, vol. 31, no. 2, pp. 2771–2778, Jan. 2007.
[21] X. Guo, F. Zheng, C. Li, X. Yang, N. Li, S. Liu, J. Wei, X. Qiu, and Q. He, "A portable sensor for *in-situ* measurement of ammonia based on near-infrared laser absorption spectroscopy," *Opt. Lasers Eng.*, vol. 115, pp. 243–248, Apr. 2019.
[22] A. Mittal, R. Soundararajan, and A. C. Bovik, "Making a 'Completely Blind' image quality analyzer," *IEEE Signal Process. Lett.*, vol. 20, no. 3, pp. 209–212, Mar. 2013.

ZHENHUA WEI received the Ph.D. degree in computer application technology from the Harbin Institute of Technology, Harbin, China, in 2005. In 2001, he joined the Harbin Institute of Technology, as a Lecturer. In 2006, he joined North China Electric Power University, Beijing, China, as a Lecturer, where he is currently an Associate Professor with the College of Control and Computer Engineering. His current research interests include the 3-D reconstruction of flame, image processing, and computer vision.

YUQI WANG was born in Shandong, China, in 1995. She is currently pursuing the master's degree in computer technology with North China Electric Power University, Beijing, China. Her research interests include computer vision, the 3-D reconstruction of flame field, and artificial intelligence applications.

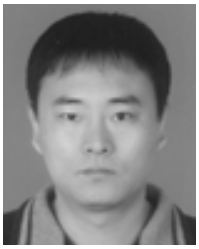

ZHIHONG LI received the B.Eng. degree from the Energy Institute, Harbin Institute of Technology, Harbin, China, in 1995, and the Ph.D. degree in engineering thermal physics from the Institute of Engineering Thermal Physics, Chinese Academy of Sciences, Beijing, China, in 2006. He is currently a Lecturer with the School of Energy Power and Mechanical Engineering, North China Electric Power University, Beijing. He was involved in advanced monitoring and characterization of fossil fuel flames. His current research interests include combustion instrumentation, multiphase flow detection, and low-quality energy utilization.

LING ZHENG received the B.Eng. degree in communication engineering and the M.Eng. degree in computer science and technology from North China Electric Power University, Beijing, China, in 1984 and 1989, respectively, where she is currently pursuing the D.Eng. degree in computer technology with the School of Control and Computer Engineering. She joined North China Electric Power University as a Professor, in 1989. Her current research interests include the 3-D reconstruction of flame field and computer vision.